



Full Text View

[Volume 29, Issue 6 \(June 1999\)](#)

Journal of Physical Oceanography

Article: pp. 1096–1108 | [Abstract](#) | [PDF \(189K\)](#)

The Relative Influence of Diapycnal Mixing and Hydrologic Forcing on the Stability of the Thermohaline Circulation*

Jubao Zhang⁺

MIT/WHOI Joint Program, Massachusetts Institute of Technology, Cambridge, Massachusetts

Raymond W. Schmitt and Rui Xin Huang

Department of Physical Oceanography, Woods Hole Oceanographic Institution, Woods Hole, Massachusetts

(Manuscript received August 12, 1997, in final form May 20, 1998)

DOI: 10.1175/1520-0485(1999)029<1096:TRIODM>2.0.CO;2

ABSTRACT

Scaling analysis of the oceanic thermohaline circulation has been done under two types of surface boundary conditions: (i) Under “relaxation” conditions (sea surface temperature and salinity are relaxed to prescribed values), there is a two-thirds power law dependence of the meridional overturning (and the poleward heat transport) on the diapycnal diffusivity. For any given external forcing, there is only one equilibrium state for the thermohaline circulation. (ii) Under “mixed” boundary conditions (temperature is relaxed to prescribed values and a virtual salt flux condition is used for salinity), multiple equilibria become possible. For a given thermal forcing, the existence of multiple equilibria depends on the relative contributions of diapycnal diffusivity and the hydrologic forcing: for each diapycnal diffusivity K , there is a threshold freshwater flux $E_c = CK^{2/3}$ (C is a constant) below which three modes are possible with one stable thermal mode, one unstable thermal mode, and a stable haline mode and above which only one stable haline mode can exist.

Numerical experiments are also implemented to test the above scaling arguments. Consistent results have been obtained under the two types of boundary conditions. The relationship derived here focuses attention on the need to better understand both the diapycnal mixing in the ocean and the strength of the hydrologic forcing at its surface.

Table of Contents:

- [Introduction](#)
- [Scaling analysis](#)
- [Numerical experiments](#)
- [Discussion and conclusions](#)
- [REFERENCES](#)
- [APPENDIX](#)
- [TABLES](#)
- [FIGURES](#)

Options:

- [Create Reference](#)
- [Email this Article](#)
- [Add to MyArchive](#)
- [Search AMS Glossary](#)

Search CrossRef for:

- [Articles Citing This Article](#)

Search Google Scholar for:

- [Jubao Zhang](#)
- [Raymond W. Schmitt](#)
- [Rui Xin Huang](#)

The thermohaline circulation plays an important role in poleward heat transport in the ocean and is thus of primary interest to climate studies. [Stommel \(1961\)](#) first recognized the possibility of multiple solutions of the thermohaline circulation. He found that under certain conditions, there could be three states possible: 1) a stable thermal mode with a relatively fast circulation, 2) a stable haline mode with a relatively slow circulation, and 3) an unstable thermal mode. [Bryan \(1986\)](#) proved the existence of multiple equilibria of the thermohaline circulation in a numerical model.

The thermohaline circulation is forced from the surface, thus the upper boundary conditions for temperature and salinity are of significance. Since there is a strong feedback between the atmospheric temperature and sea surface temperature (SST), a relaxation condition for the SST has been widely used ([Haney 1971](#)):

$$K \frac{\partial T}{\partial z} = \Gamma(T^* - T_s), \quad (1)$$

where T^* is the “apparent atmospheric temperature” determined by the sum of solar insolation, back radiation, latent and sensible heat fluxes; T_s is SST; and Γ is inverse of the relaxation time. The strong feedback mechanism allows the SST to be maintained around the prescribed T^* .

For salinity, there are several choices. First we can relax the sea surface salinity to a prescribed distribution, analogous to temperature:

$$K \frac{\partial S}{\partial z} = \Gamma_s(S^* - S_s). \quad (2)$$

This condition is very easy to use, but it is hardly justified physically because there is no such feedback between S^* and S_s . Instead, the salinity is related to the SST, which affects the evaporation rate at the sea surface. The second way is to use a virtual salt flux condition for salinity:

$$K \frac{\partial S}{\partial z} = (e - p)\bar{S}, \quad (3)$$

where $e - p$ is evaporation minus precipitation, including runoff, and \bar{S} is the averaged salinity at the surface. This condition is an approximation to the freshwater flux condition, and increasing numbers of ocean models use this boundary condition for salinity in studies of the thermohaline circulation. [Huang \(1993\)](#) proposed a more realistic upper boundary condition, the so-called “natural” boundary condition on salinity. Due to the restraint of the free surface requirement, this kind of boundary condition is not discussed here, but in terms of the scaling argument below it should be similar to the virtual salt flux case. For simplicity, wind stress effects are neglected in the scaling argument and in most of the numerical experiments. We call the combination of [\(1\)](#) and [\(2\)](#) “relaxation” boundary conditions and, in comparison, [\(1\)](#) and [\(3\)](#) are called “mixed” boundary conditions.

The importance of the diapycnal diffusivity to the thermohaline circulation under the relaxation boundary conditions has been discussed and widely examined in numerical models. [Welander \(1971\)](#) derived a scaling relationship for the zonal flow based on a vertical advective–diffusive balance and the thermal wind relation. [Bryan \(1987\)](#) postulated this to hold for the zonally averaged meridional flow as well; that is, the meridional overturning should have a two-thirds power law dependence on the diapycnal diffusivity, even though he only observed an approximate one-third power law in his numerical experiments. [Marotzke \(1997\)](#) restrained the diapycnal diffusivity to act only at lateral boundaries and in convection regions and found that, when the vertical diffusivity K is below $30 \text{ cm}^2 \text{ s}^{-1}$, the meridional overturning strength is proportional to $K^{2/3}$. He offered a theory to get the relation between the north–south density difference and the east–west density difference, and the latter is directly related to the shear of meridional flow and thus the thermohaline circulation. The relation between zonal and meridional density gradients can also be found in [Hovine and Fichefet \(1994\)](#).

The thermohaline circulation under mixed boundary conditions has also been investigated ([Weaver et al. 1993](#); [Weaver and Hughes 1992](#); [Rahmstorf et al. 1996](#)). [Weaver et al. \(1993\)](#) examined the effect of freshwater fluxes on the stability and variability of the thermohaline circulation. They found that the freshwater forcing is the dominant factor in determining stability and internal variability. Increasing the relative importance of the freshwater flux versus thermal forcing caused, in turn, one stable steady state of the model, two stable states, one stable and one unstable equilibrium, or no stable steady states at all. In addition, [Huang and Chou \(1994\)](#) studied the parameter sensitivity of the saline circulation forced by freshwater flux alone. When the freshwater flux is increased from 0.01 to 1 m yr^{-1} with other parameters fixed, the system evolves from a steady state with no oscillations to a state of periodic oscillation whose frequency increases almost linearly

with the amplitude of the freshwater flux. On the other hand, when the freshwater flux is fixed and the vertical mixing coefficient is increased from 0.5 to $2.5 \text{ cm}^2 \text{ s}^{-1}$, the system evolves from a steady state to a state of single-period oscillation, to a chaotic state, to a single period state, and finally, when the vertical mixing is larger than $2.0 \text{ cm}^2 \text{ s}^{-1}$, to another chaotic state.

These studies suggest that the freshwater flux and the diapycnal diffusivity are very important parameters to the thermohaline circulation, yet both are poorly known from observations. In the following scaling analysis and numerical experiments we attempt to understand the sensitivity of the thermohaline circulation to these two parameters. In [section 2](#), the scaling analyses of the thermohaline circulation under two different kinds of upper boundary conditions are provided. In [section 3](#) numerical experiments are implemented to compare with the scaling results. [Section 4](#) contains a summary and discussion.

2. Scaling analysis

a. Equations

Similar to [Welander \(1971\)](#), we start from the following equations:

(i) the incompressibility condition

$$\frac{\partial u}{\partial x} + \frac{\partial v}{\partial y} + \frac{\partial w}{\partial z} = 0, \quad (4)$$

(ii) the thermal wind relation

$$\frac{\partial \mathbf{u}}{\partial z} = -\frac{g}{\rho_0 f} \mathbf{k} \times \nabla \rho, \quad (5)$$

(iii) the vertical advective–diffusive balance of density

$$w \frac{\partial \rho}{\partial z} = K \frac{\partial^2 \rho}{\partial z^2}, \quad (6)$$

where $\mathbf{u} = u\mathbf{i} + v\mathbf{j}$ and w are the horizontal and vertical components of velocity respectively, f is the Coriolis parameter, ρ is the density, K is the assumed uniform diapycnal diffusivity of density, and g is the gravitational acceleration.

Assumption (i) is used widely in oceanic theoretical and numerical studies, and (ii) comes from the geostrophic and hydrostatic relations, which are true for the large-scale thermohaline circulation. Assumption (iii) has been invoked by [Munk \(1966\)](#) and justified by the correspondence of observed vertical profiles of salinity and temperature to the model (depth between 1 and 5 km); in addition, [Munk and Wunsch \(1998\)](#), hereafter MW) have revisited this issue. This assumption was used in the scaling argument of [Welander \(1971\)](#) and [Bryan \(1987\)](#).

From the above equations, we obtain the scaling relations:

$$\begin{aligned} UD &= WL, \\ \frac{\Delta \rho}{\rho_0} &= \frac{fUL}{gD}, \\ D &= \frac{K}{W}, \end{aligned} \quad (7)$$

where $U(L)$ and $W(D)$ are horizontal and vertical velocity (length) scales, respectively, and $\Delta \rho$ is the north–south density difference at the ocean surface.

From these we can derive the vertical length scale in terms of $\Delta \rho/\rho_0$:

$$D = \left[\frac{fKL^2}{g\Delta\rho/\rho_0} \right]^{1/3}, \quad (8)$$

which is actually the scale thickness of the thermocline ([Samelson and Vallis 1997](#)).

Thus, the strength of the meridional overturning is

$$M = UDL = WL^2 = \left[\frac{g\Delta\rho K^2 L^4}{\rho_0 f} \right]^{1/3}. \quad (9)$$

Note that M is determined by the meridional velocity \mathbf{v} , which is related to the east–west density difference, rather than the north–south density difference. Since in the thermocline, the velocity components u and \mathbf{v} are of the same order and u is determined by the north–south density difference, we infer that \mathbf{v} has the same order of magnitude. [Marotzke \(1997\)](#) provides a discussion, in which the east–west density difference is closely related to the north–south surface density difference. However, he assumed vertical mixing only occurs in the lateral boundary regions, which is different from the uniform mixing assumed here. To the lowest order, we can assume that (9) is an acceptable estimate for the strength of the meridional overturning cell.

The poleward heat transport is very important for climate studies. This can be scaled as follows:

$$Q = C_0 \rho_0 c_p M \Delta T \propto K^{2/3}, \quad (10)$$

where c_p is the specific heat under constant pressure and the north–south temperature difference ΔT is used to represent the temperature difference between the deep flow and the surface return flow. We use both maximum M and ΔT to estimate Q ; however, in the real ocean (a single-hemisphere basin), maximum M occurs with minimum ΔT and maximum ΔT lies in the minimum M region. As a result, the maximum poleward heat transport is found in midlatitudes. Thus, a constant factor C_0 is introduced here to represent this effect. For the simplest case, we can assume that Q reaches its maximum at midlatitudes where both ΔT and M are assumed half of their maximum values; thus we could expect an approximate value of $C_0 = 1/4$.

Furthermore, assuming a linear equation of state

$$\rho = \rho_0(1 - \alpha T + \beta S), \quad (11)$$

then the ratio $\Delta\rho/\rho_0$ in (8) and (9) can be replaced by

$$\Delta\rho/\rho_0 = |\alpha\Delta T - \beta\Delta S|, \quad (12)$$

where ΔT and ΔS are north–south temperature and salinity differences.

b. Relaxation boundary conditions

In most cases using relaxation boundary conditions in the literature, both Γ and Γ_s are quite large so that ΔT and ΔS can be approximated by ΔT^* and ΔS^* . This assumption will be used in the following analysis.

We find it useful to define the horizontal density ratio:

$$R = \frac{\beta\Delta S}{\alpha\Delta T}. \quad (13)$$

In present-day oceans, the water is cold and fresh in polar regions, and warm and salty in equatorial regions; thus temperature and salinity have opposite effects on the surface density difference. When $R < 1$, the temperature dominates the density difference, and the densest water is formed and sinks in the polar regions. The thermohaline circulation is in the

“thermal” mode. In contrast, when $R > 1$, the salinity dominates the density difference, and the densest water is formed and sinks in the equatorial regions. This thermohaline circulation is in the “haline” mode.

Using (13), the depth scale and meridional overturning scalings become

$$D = \left[\frac{fKL^2}{g\alpha\Delta T|R-1|} \right]^{1/3}, \quad (14)$$

$$M = \left[\frac{g\alpha\Delta T|R-1|K^2L^4}{f} \right]^{1/3}. \quad (15)$$

With the relaxation boundary conditions, ΔT and ΔS are very close to the constant ΔT^* and ΔS^* . As a result, the north-south density difference is nearly fixed, so there is only one thermohaline circulation mode. The above power laws have been discussed previously (Welander 1971; Bryan 1987) and are reproduced here as a first step for the case under mixed boundary conditions. In addition, the above conclusions will be examined in a numerical model in section 3b.

c. Mixed boundary conditions

1) NORTH-SOUTH SALINITY DIFFERENCE

Under mixed boundary conditions (1) and (3), the north-south salinity difference is no longer fixed; instead, it becomes part of the solution we are pursuing.

Consider a two-box model of the ocean (Stommel 1961), in which a polar box and an equatorial box are well mixed and connected by pipes at the top and the bottom. Defining \bar{S}_e and \bar{S}_p as salinities in the equatorial and polar boxes respectively, the salt conservation equations are

$$\dot{\bar{S}}_e = \frac{\bar{E}_e \bar{S}}{H} - \frac{M_0}{HL^2/2} (\bar{S}_e - \bar{S}_p), \quad (16)$$

$$\dot{\bar{S}}_p = \frac{\bar{E}_p \bar{S}}{H} + \frac{M_0}{HL^2/2} (\bar{S}_e - \bar{S}_p), \quad (17)$$

where \bar{E}_e, \bar{E}_p are the evaporation minus precipitation rates in the equatorial and polar box, L^2 is the horizontal area of the ocean basin, M_0 is the volume flux between the two boxes, H is the depth of the ocean, \bar{S} is the averaged salinity over the whole basin, and an overdot denotes the time derivative.

From the above two equations, we can derive an equation governing evolution of the salinity difference, $\Delta \bar{S}_1 = \bar{S}_e - \bar{S}_p$,

$$\Delta \dot{\bar{S}}_1 = \frac{4}{H} \left(\frac{\bar{E}_e - \bar{E}_p}{4} \bar{S} - \frac{M_0}{L^2} \Delta \bar{S}_1 \right). \quad (18)$$

To get a more reasonable estimate of the north-south salinity difference in the scaling analysis, we make the following assumptions:

$$\Delta S = 2\Delta S_1, \quad (19)$$

$$E_e - E_p = 2(\bar{E}_e - \bar{E}_p), \quad (20)$$

$$M = 2M_0, \quad (21)$$

where ΔS , $E_e - E_p$, and M are used to represent the corresponding quantities in more complicated models, like numerical models, rather than that from a two-box model that is strongly averaged. The above extension from a box model to a more realistic model is based on simple linear assumptions, which may differ from the real situation, but as a scaling argument, we believe it reflects the lowest order approximation. Thus, $\Delta S (E_e - E_p)$ is the salinity (freshwater) difference between northern and southern regions, and M is the maximum of the meridional overturning. For convenience, we introduce

$$E = (E_e - E_p)/2 \quad (22)$$

to represent the magnitude of freshwater forcing. Then we have

$$\Delta \dot{S} = \frac{2}{H} \left(E \bar{S} - \frac{M}{L^2} \Delta S \right). \quad (23)$$

For a steady state, we obtain

$$\begin{aligned} \Delta S_0 &= \frac{EL^2}{M} \bar{S} \\ &= \frac{\bar{S}E}{W} \\ &= \frac{\bar{S}ED}{K}. \end{aligned} \quad (24)$$

A similar scaling result has been obtained in [Huang and Chou \(1994\)](#). We can see that ΔS_0 is proportional to the magnitude of the freshwater forcing and inversely proportional to the strength of the meridional overturning circulation rate.

2) SCALING ANALYSIS AND SOLUTIONS

With ΔS_0 given in [\(24\)](#), we obtain

$$\frac{\Delta \rho}{\rho_0} = \left| \alpha \Delta T - \frac{\beta \bar{S}ED}{K} \right|. \quad (25)$$

From here we can conclude that, when

$$\alpha \Delta T > \frac{\beta \bar{S}ED}{K}, \quad (26)$$

the density difference is thermally dominant. Alternatively, when the thermal effect is less than the saline effect, the density difference is salt dominant.

Substituting [\(25\)](#) into [\(8\)](#), we obtain a quartic equation for D

$$\frac{fL^2K}{gD^3} = \left| \alpha \Delta T - \frac{\beta \bar{S}ED}{K} \right|. \quad (27)$$

Since the salinity difference is now related to the vertical length scale, the relation between the depth scale and the external parameters becomes more complicated.

Introducing the following nondimensional variables,

$$F = \frac{fL^2}{g\alpha\Delta T} \left(\frac{\beta\bar{S}}{\alpha\Delta T} \right)^3 \frac{E^3}{K^2}, \quad (28)$$

$$R = \frac{\beta\bar{S}ED}{\alpha\Delta TK}, \quad (29)$$

Eq. (27) becomes

$$|R^4 - R^3| = F. (30)$$

Using (24), R can be written as

$$R = \frac{\beta\Delta S_0}{\alpha\Delta T}, \quad (31)$$

which is the horizontal density ratio representing the relative contributions of salt and heat to the surface density. When $R < 1$, the thermal forcing dominates, and we have thermal modes; on the other hand, when $R > 1$, the freshwater forcing dominates, and we obtain a haline mode.

In the limits of $R \ll 1$, Eq. (30) reduces to the $K^{2/3}$ power law dependence of meridional overturning on diapycnal diffusivity found under the relaxation boundary conditions. If $R \gg 1$, the Huang and Chou (1994) $K^{1/2}$ power law dependence of meridional overturning upon diapycnal diffusivity for the saline circulation (freshwater forcing only) is recovered.

The general solution of Eq. (30) can be obtained through the following two cases:

(i) Thermal mode(s) equation ($R < 1$)

$$R^4 - R^3 + F = 0. (32)$$

(ii) Haline mode(s) equation ($R > 1$)

$$R^4 - R^3 - F = 0. (33)$$

The solution(s) can be found in the appendix.

The nature of the solution to Eq. (30) depends on the size of F relative to a critical parameter:

$$F_c = \frac{3^3}{4^4} = \frac{27}{256}. \quad (34)$$

When $F < F_c$, two thermal modes and one haline mode are possible; when $F > F_c$, only one haline mode can exist.

The above solutions are based on R , and then we can calculate the meridional overturning by (9) and the poleward heat transport by (10).

Assuming the thermal forcing is fixed ($\Delta T = \text{const}$), (34) implies a critical value for the freshwater forcing:

$$E_c(K) = \sqrt[3]{\frac{27g\alpha\Delta T}{256fL^2} \frac{\alpha\Delta T}{\beta\bar{S}}} K^{2/3} \quad (35)$$

$$= CK^{2/3}. \quad (36)$$

Thus, for a given value of K , there is an upper limit of freshwater forcing $E_c(K)$ beyond which no thermal mode can exist. Below this value two thermal modes, in addition to the haline mode, are possible for all given conditions.

The reason for such an upper limit on the thermal mode can be understood as follows. The freshwater forcing acts as a brake on the thermally driven overturning circulation. For example, with $E > 0$, we know the maximum meridional overturning is smaller than that without freshwater forcing, that is,

$$M < \left[\frac{g\alpha\Delta TL^4 K^2}{f} \right]^{1/3} = M_{\text{Th}}, \quad (37)$$

where M_{Th} is the meridional overturning due to thermal forcing alone. Using (24),

$$\begin{aligned} \Delta S_0 &= \frac{L^2 \bar{S}}{M} E, \\ &> \frac{L^2 \bar{S}}{M_{\text{Th}}} E. \end{aligned} \quad (38)$$

For a given thermal forcing ΔT , ΔS_0 increases with larger E ; thus, when E is large enough, ΔS_0 can overcome the density effect of ΔT , making the thermal mode impossible.

We plot the critical line (36) in Fig. 1. In the region below the critical curve three modes are possible: two thermal modes and one haline mode, while in the region above it only one haline mode can exist.

Also, we plot the dependence of the meridional overturning on E and K , respectively (Fig. 2). The upper solid line corresponds to the stable thermal mode, while the lower solid line is the solution for the haline mode, and the dotted line represents the result for the unstable thermal mode. For $K = 1 \text{ cm}^2 \text{ s}^{-1}$ (Fig. 2), there is a bifurcation point at about $E = 1 \text{ m yr}^{-1}$ beyond which only one haline mode is possible.

The above arguments are based on the assumption of a specified equator–pole temperature difference. However, since the atmosphere and oceans constitute a coupled system, the temperature difference ΔT could change. From (35), a change in ΔT will lead to a different critical relation between diapycnal diffusivity and hydrologic forcing. Past climatic states of the earth may have had significantly different ΔT and E , and both must be considered in evaluating the possible modes of the thermohaline circulation.

3) STABILITY ANALYSIS

Next we analyze the stability of the solutions obtained above. We separate ΔS into two parts:

$$\Delta S = \Delta S_0 + \Delta S', \quad (39)$$

where ΔS_0 is the steady solution and $\Delta S'$ is a small perturbation. Similarly, we assume the meridional overturning will change correspondingly:

$$M = M_0 + M'. \quad (40)$$

From Eq. (9), we derive

$$\frac{M'}{M_0} = -\frac{1}{3} \frac{\beta \Delta S'}{\alpha \Delta T - \beta \Delta S_0}. \quad (41)$$

By substituting (39) and (41) into (23), we obtain

$$\Delta \dot{S}' = A \Delta S', \quad (42)$$

where

$$A = \frac{2(4R - 3) M_0}{3(1 - R) HL^2}. \quad (43)$$

For the thermal mode with $\frac{3}{4} < R < 1$, $A > 0$, and thus this mode is unstable. In comparison, for the other thermal mode, which has $R < \frac{3}{4}$, and for the haline mode, which corresponds to $R > 1$, we have $A < 0$, so both modes are stable solutions.

4) APPLICATION TO NORTH ATLANTIC AND NORTH PACIFIC

The above scaling argument is based upon a square basin. In fact, for a rectangular basin (i.e., $L_x \neq L_y$), we can replace the horizontal area L^2 by $L_x L_y$.

Given the uncertainty associated with both the diapycnal diffusivity and $e - p$ over the oceans, it is unrealistic to compare the current scaling argument with the real oceans in any detail. However, a rough estimate can be made based on presently available information. A map of evaporation minus precipitation over the global ocean is plotted in [Fig. 2](#) of [Schmitt \(1995\)](#) and is used for the estimate of $e - p$. Here we focus on the Northern Hemisphere where the North Atlantic and North Pacific are isolated and most appropriate for our scaling argument. Due to the effect of the intertropical convergence zone, there is more precipitation than evaporation in the equatorial region, thus the maximum $e - p$ lies near 15°N for the North Atlantic and 20°N for the North Pacific. The minimum $e - p$ (or maximum $p - e$) lies in the polar region of both oceans, close to 60°N . As an approximation, we take $L_y = 5 \times 10^6$ m for both oceans and $L_x = 6 \times 10^6$ m for North Atlantic and $L_x = 12 \times 10^6$ m for North Pacific. Then we estimate ΔT and \bar{S} for both oceans from the [Levitus \(1982\)](#) climatology between the maximum and minimum $e - p$ regions, respectively. We obtain approximate values of $\Delta T = 18^\circ\text{C}$, $\bar{S} = 36$ psu for the North Atlantic and $\Delta T = 20^\circ\text{C}$, $\bar{S} = 34$ psu for the North Pacific.

Compared to $e - p$, the diapycnal diffusivity is perhaps even less well known. Recent observations indicate strong spatial variability of diapycnal mixing in the oceans. [Ledwell et al. \(1993\)](#) found that the diapycnal diffusivity is about $0.15 \text{ cm}^2 \text{ s}^{-1}$ in the upper thermocline in a tracer release experiment, while the diapycnal diffusivity is much larger close to rough topography in the abyss (approaches $100 \text{ cm}^2 \text{ s}^{-1}$; [Toole et al. 1994](#); [Polzin et al. 1997](#)). The basin-scale budget estimates require an averaged diapycnal diffusivity of about $1 \text{ cm}^2 \text{ s}^{-1}$ ([Munk 1966](#); MW). For simplicity, we adopt the canonical value of $K = 1 \text{ cm}^2 \text{ s}^{-1}$ for both basins in the scaling estimate here; however, the uncertainty of this value should be emphasized.

Using the above parameters, we estimate the critical evaporation minus precipitation rate as

$$E_{c\text{NA}} = 0.92 \text{ m yr}^{-1} \quad (44)$$

for the North Atlantic Ocean and

$$E_{c\text{NP}} = 0.89 \text{ m yr}^{-1} \quad (45)$$

for the North Pacific Ocean. The critical values of freshwater forcing are surprisingly close for both oceans.

From the [Schmitt \(1995\)](#) global ocean $e - p$ map, we find E_{NA} is about 0.75 m yr^{-1} for the North Atlantic Ocean and E_{NP} is about 1.05 m yr^{-1} for the North Pacific Ocean. Thus, the estimated freshwater forcing is much stronger in the North Pacific than in the North Atlantic. Since $E_{\text{NA}} < E_{c\text{NA}}$, the scales suggest that the North Atlantic Ocean is in the multiple equilibria regime. Presently, the North Atlantic Deep Water (NADW) is formed in the polar region and exported equatorward, characteristic of a thermal mode. In contrast, for the North Pacific, since $E_{\text{NP}} > E_{c\text{NP}}$, only the haline mode is possible by the scaling argument. This is in line with the lack of deep-water formation in the Pacific polar regions. The results are summarized in [Table 1](#).

[Warren \(1983\)](#) noted the effects of low sea surface temperature on the diminution of evaporation and suggests that this causes the lack of bottom-water formation in the Pacific compared to the North Atlantic. Here we find it is also possible that the larger gradient of $e - p$ in the North Pacific inhibits a thermal-mode overturning cell. The stronger freshwater forcing and lower critical E value for the North Pacific both favor the single haline mode. Compared to the North Atlantic Ocean, even though the higher north-south temperature gradient and lower mean salinity act to increase the critical E value, the large size in the zonal dimension surpasses the above effects and leads to a smaller critical value in the North Pacific than the

North Atlantic. Thus, it is easier to enter the haline mode even with the same freshwater forcing. In addition, there could well be significant differences in diapycnal mixing rates in the two basins due to varying bathymetry and tidal forcing (Polzin et al. 1997; MW).

The individual oceans, however, are not isolated systems; moreover there is interaction between the oceans and the atmosphere. As a result, there is strong feedback between ΔT , E , and the strength of the thermohaline circulation. Thus, parameters ΔT , E , etc. are not givens, but rather are part of the solution of the more complicated coupled system. Hopefully, the simple scaling argument given here provides the lowest order estimate of the behavior of the thermohaline circulation. Based upon the rough observations available, it is consistent with the current oceanic situation.

5) COMPARISON WITH BOX MODEL RESULTS

Marotzke (1990) used a two-box model similar to Stommel (1961), in which he defined the following nondimensional variables:

$$F_M = \frac{\beta H_S}{K_M (\alpha \Delta T)^2},$$

$$R_M = \frac{\beta \Delta S}{\alpha \Delta T},$$

where H_S is the equivalent salt flux, and K_M is the linear proportionality coefficient between the interbox flow and the density difference. He found for $F_M < 0.25$, three steady states exist, including one haline mode and two thermal modes. For $F_M > 0.25$, only one haline mode is possible. In addition, for $R_M < 0.5$ or $R_M > 1.0$, the solution is stable, and for $0.5 < R_M < 1.0$, the solution is unstable. Therefore, in the multiple equilibria region ($F_M < 0.25$), there is one stable thermal mode, one unstable thermal mode, and one stable haline mode, and when $F_M > 0.25$, there is only one stable haline mode.

Huang et al. (1992) studied the structure and stability of the multiple equilibria of the thermohaline circulation using 2×2 and 3×2 box models. They defined the following nondimensional number

$$p = \frac{\Gamma(e - p)}{\rho_0 c_p}, \quad (46)$$

where Γ is the Rayleigh relaxation coefficient. In the 2×2 box model, for $0 < p < p_c$, three solutions exist: one stable thermal mode, one unstable thermal mode, and one stable haline mode; for $p > p_c$, only one stable haline mode exists. Here p_c is the nondimensional critical freshwater forcing. Note the similarity between the upper panel of Fig. 2 in this article and Fig. 5 in Huang et al (1992).

Our scaling analysis is consistent with the above box models in the following aspects: under certain conditions, three solutions are possible, which include one stable thermal mode, one unstable thermal mode, and one stable haline mode; otherwise only one stable haline mode is possible. Compared to Marotzke (1990), the criteria on $R (= \beta \Delta S_0 / \alpha \Delta T)$ for the stability is different, we get an unstable solution for $0.75 < R < 1$ through the scaling argument, which corresponds to the range $0.5 < R < 1$ in Marotzke (1990). As in Marotzke (1990) and Huang et al. (1992), we obtain an upper limit of the freshwater forcing (or equivalent salt flux) beyond which no steady thermal mode is found.

In contrast to the box models, we include the Coriolis parameter, basin dimensions, and more importantly the two uncertain variables: diapycnal diffusivity and freshwater forcing. For a given set of parameters, the scaling analysis permits an estimate of how the thermohaline circulation will behave, which is unattainable with the box models. The role of freshwater forcing has been studied extensively in the box models, but the effect of diapycnal diffusivity cannot be examined due to the strong numerical diffusion intrinsic to these models.

3. Numerical experiments

a. Model description

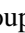
Experiments utilizing the GFDL MOM2 were conducted to explore the validity of the scaling arguments in [section 2](#). The details of the model can be found in [Bryan \(1969\)](#) and [Pacanowski \(1995\)](#). The special features of these experiments are as follows.


The model domain is a sector basin of $60^\circ \times 60^\circ$, and the horizontal resolution is 3.75° . There are 15 levels vertically, with thickness from 50 m at the top to 500 m at the bottom; the total depth is 4500 m.

The horizontal and vertical momentum viscosity coefficients are $A_h = 1.0 \times 10^6 \text{ m}^2 \text{ s}^{-1}$ and $A_v = 20 \text{ cm}^2 \text{ s}^{-1}$, respectively. For the tracer equations, the eddy transport parameterization of [Gent and McWilliams \(1990\)](#) and isopycnal/diapycnal mixing is used, and no background horizontal diffusion is needed. We take $K_{\text{ISO}} = K_{\text{ITD}} = 500 \text{ m}^2 \text{ s}^{-1}$, where K_{ISO} is the isopycnal diffusion coefficient and K_{ITD} is the downgradient diffusivity of the isopycnal thickness.


Diapycnal (vertical) diffusivity is the key factor in the experiments, and is varied from 0.1 to $5 \text{ cm}^2 \text{ s}^{-1}$.

b. Relaxation boundary conditions

The first layer temperature and salinity are relaxed to the SST and SSS climatology ([Levitus 1982](#)) with a relaxation time of 30 days (see [Fig. 3](#) ). Two groups of experiments were implemented, one group without any wind stress and in the other the zonally averaged annual climatological surface wind stress of [Hellerman and Rosenstein \(1983\)](#) is used. In both groups of experiments, diapycnal diffusivities were 0.1, 0.25, 0.5, 1.0, 2.0, and $5.0 \text{ cm}^2 \text{ s}^{-1}$ with all other parameters fixed. The $0.1 \text{ cm}^2 \text{ s}^{-1}$ experiments were run for 12 000 years, the $5.0 \text{ cm}^2 \text{ s}^{-1}$ experiments are run for 4000 yr, and all others 8000 years. Equilibria were reached in each experiment (with the surface averaged upward heat flux oscillating less than about 0.05 W m^{-2}).

The experiments with and without wind stress are consistent with the scaling argument ([Fig. 4](#) ). When the diapycnal diffusivity is very small, wind stress plays an increasingly important role in the thermohaline circulation since the penetration depth forced by the wind stress becomes greater than that caused by buoyancy effects. In contrast, when the diapycnal diffusivity is as large as $0.5 \text{ cm}^2 \text{ s}^{-1}$, the wind stress makes almost no difference to the thermohaline circulation under the relaxation boundary conditions.


When [Bryan \(1987\)](#) examined the sensitivity of the thermohaline circulation to the vertical diffusivity, he derived the two-thirds power law through scaling arguments, but only got an approximate one-third power law dependence in the numerical experiments. One reason is that the experiments were run only to 1200 years, which, for most of the experiments, is not long enough to reach equilibrium. In addition, the diapycnal mixing due to the action of the horizontal diffusivity on sloping isopycnals could also affect the thermohaline circulation. [Wright and Stocker \(1992\)](#) used a two-dimensional (vertical–meridional) model to examine the sensitivity of the thermohaline circulation to the vertical diffusivity. For the North Atlantic Ocean, they found $M \propto K^{1/3}$ with wind stress and $M \propto K^{1/2}$ without wind stress. Their model applied to the Pacific and the Indian Oceans obtained $M \propto K^{2/3}$. [Marotzke \(1997\)](#) restricted all vertical mixing to the boundaries and found $M \propto K^{2/3}$. Here we obtain the two-thirds power law dependence in a three-dimensional OGCM with uniform vertical mixing.

The poleward heat transports in the above numerical experiments are plotted in [Fig. 5](#) . Note that a least square method fitting of the numerical experiments gives

$$C_0 = \frac{1}{3}, \quad (47)$$

which is used in the scaling argument given in [\(10\)](#). We can see that an approximate two-thirds power law dependence is obtained, as given in the scaling argument, for the case without wind stress. For the case with wind stress, especially in the low diffusivity experiments, the Ekman cells, driven by the wind stress, can carry a portion of the total poleward heat flux. As a result, the experimental results deviate from the two-thirds power. Note, however, that the two-thirds power law in the poleward heat transport is not as close as in the meridional overturning.

One significant difference between the model formulation here and the earlier work ([Bryan 1987](#); [Wright and Stocker 1992](#); [Marotzke 1997](#)) is the inclusion of the [Gent and McWilliams \(1990\)](#) isopycnal tracer mixing scheme, which eliminates the false diapycnal diffusivities caused by horizontal diffusion, especially in places where the slope of the isopycnals is large, like western boundary current and convection regions. We believe this explains why the meridional overturning so closely obeys the two-thirds power law dependence on the vertical diffusivity derived in the scaling analysis.

Here we use a relaxation condition for temperature (same as in the upper panel of [Fig. 3](#) ) and a virtual salt flux boundary condition for the salinity with a simple “linear” profile of evaporation minus precipitation. No wind stress is applied. The freshwater forcing is defined for a basin confined between the equator $\Phi = 0$ and a northern boundary $\Phi = \Phi_n$ by the expression

$$e - p = \frac{W_0}{\cos\phi} \left(1 - \frac{2\phi}{\phi_n} \right), \quad (48)$$


then the maximum and minimum of $e - p$ are W_0 (at $\Phi = 0$) and $-2W_0$ (at $\Phi = \Phi_n = 60^\circ$), respectively; therefore, we have


$$E = 1.5W_0 \quad (49)$$

to represent the magnitude of the freshwater forcing, as defined in the scaling argument. This E will be used in the scaling estimate for comparison with the numerical experiments. When $E > 0$, the freshwater forcing opposes the thermal forcing; when $E < 0$, polar water is salty, deep water can form only close to the northern wall, and we obtain only the thermal mode.

Three groups of hysteresis experiments are shown, with $K = 0.3, 0.5,$ and $1.0 \text{ cm}^2 \text{ s}^{-1}$. In order to find the bifurcation point of the freshwater forcing, we first run the model to an equilibrium with $E \leq 0$. From there we increased E very slowly (0.1 or 0.05 m yr^{-1} per thousand years). Due to the slow rate of change of the forcing, the model remains in quasi equilibrium, and we can see the response of the model to the different freshwater forcings while the thermal forcing is basically fixed.

For each group of experiments, there is an upper limit of E beyond which the thermal mode does not exist. If we continue to increase the freshwater forcing past this point, the thermohaline circulation will stay in the haline mode. When we decrease E starting from a haline mode, the ocean stays in the mode until flushing, a phenomenon peculiar to the haline mode, occurs. In the numerical runs, the model cannot reach equilibrium in the haline mode. Over a long period, the polar deep ocean becomes warmer and saltier. With cold and fresh water overlying the warm and salty deep water in the polar basin, an instability sets in and very strong convection occurs, which releases the heat accumulated for hundreds or thousands of years ([Marotzke 1990](#); [Huang 1994](#)). However, even with flushing we can see that under certain conditions, there are two modes possible: one thermal mode and one haline mode, which is consistent with the scaling and stability analysis.

In order to gain confidence in the quasi-equilibrium effects displayed in the above experiments, we conducted a series of experiments, where $K = 0.5 \text{ cm}^2 \text{ s}^{-1}$ and with different values of E . We start the first experiment from $E = -0.15 \text{ m yr}^{-1}$ and an initially homogeneous state. After 4000 years of integration, we obtained a quasi equilibrium. We start the next experiment from this final state with another E and run it to another equilibrium. When the E is large enough, the upper limit of the freshwater forcing is passed and the ocean enters a haline mode. Since there is no steady equilibrium for a haline mode, we run the model for at least one flushing period; that is, we stop the experiment in the haline mode after at least one flushing event. Then we begin to decrease E to a specified value and continue our experiments. The results are plotted in [Fig. 6](#)  (the “○” points in the figure). We can see that they are pretty close to the quasi-equilibrium experiments and we obtained two modes for a value of $E = 0.45 \text{ m yr}^{-1}$.

Through the above experiments, we find that for each K , there is an upper limit on E for the existence of a stable thermal mode below which two modes are possible, as predicted by the scaling analysis. We plot the different critical E versus diapycnal diffusivity in [Fig. 7](#) . The numerical experiments are consistent with the scaling argument, though quantitatively there is a difference. The linear equation of state assumed in the scaling argument could cause such a distortion since the full state equation used in the numerical models is highly nonlinear (the thermal expansion coefficient α is a strong function of temperature). Convection plays an essential role in deep-water formation and the top-to-bottom density difference is important for convection. Thus, it is crucial to determine the role of temperature and salinity in the vertical density distribution in the convection region. For the thermal mode, convection occurs in the polar region where the temperature is low and, thus, α is small (about $1.0 \times 10^{-4} \text{ K}^{-1}$ at 4°C); since we use a universal value $2.0 \times 10^{-4} \text{ K}^{-1}$ in the scaling, the magnitude of the meridional overturning for the thermal mode, as well as the magnitude of the critical freshwater flux, are overestimated.

concluded that the freshwater forcing is the dominant factor in determining the model's stability and internal variability. Increasing the relative importance of freshwater fluxes versus thermal forcing led to, in turn, one stable steady state of the model, two stable states, one stable, and one unstable equilibrium, or no stable steady states. If the freshwater forcing is sufficiently strong, self-sustained oscillations exist in the deep-water formation rate, which last thousands of years. We can find the transition from a multiequilibria region to a single haline mode region when we increase the magnitude of the freshwater forcing, and this is basically consistent with our scaling argument. However, in contrast to [Weaver et al. \(1993\)](#), the criteria to determine the behavior of the thermohaline circulation is a nondimensional number defined by [\(28\)](#), which includes not only the freshwater forcing versus thermal forcing, but also the effect of diapycnal diffusivity and the dimensions of the basin. For a given basin, the diapycnal diffusivity also determines the behavior of the thermohaline circulation. [Weaver et al. \(1993\)](#) investigated the use of different vertical diffusivities. In one experiment a value of $K = 0.5 \text{ cm}^2 \text{ s}^{-1}$ was set throughout the water column, in another K was made to increase from $0.3 \text{ cm}^2 \text{ s}^{-1}$ at the surface to $1.3 \text{ cm}^2 \text{ s}^{-1}$ at the bottom of the model ocean. No major differences were observed. However, from [Cummins et al. \(1990\)](#), we deduce that the value of diapycnal diffusivity in the thermocline is more important than that in the deep ocean. As the above two values of vertical diffusivity are very close, it is not surprising that Weaver et al. saw little difference, as far as the behavior of the thermohaline circulation is concerned, even though the T - S structure in the deep ocean could be very different. As suggested by the scaling analysis and the numerical experiments presented here, not only the freshwater forcing but also the diapycnal diffusivity play important roles in determining the stability and variability of the thermohaline circulation under mixed boundary conditions.

[Rahmstorf \(1995\)](#) investigated the sensitivity of the North Atlantic thermohaline circulation to the input of freshwater using a global ocean circulation model coupled to a simplified atmospheric model. In his experiments, moderate changes in freshwater input induced transitions between different equilibrium states, leading to substantial changes in regional climate. His experiments provide a map of the equilibrium states and bifurcation points of the Atlantic thermohaline circulation as a function of freshwater flux. The saddle-node bifurcation first described by [Stommel \(1961\)](#) is confirmed in the [Rahmstorf \(1995\)](#) experiments. Beyond the bifurcation point, the North Atlantic Deep Water (NADW) circulation cannot be sustained. Below the bifurcation point, at least two states are found: one is characterized by the absence of NADW, one with NADW. Qualitatively, the experiments in [Rahmstorf \(1995\)](#) are consistent with the scaling analysis in this article. In addition, given the sensitivity of thermohaline circulation to the diapycnal diffusivity deduced in the present scaling argument, it is highly likely that the bifurcation point in the coupled GCM will be sensitive to the diapycnal (vertical) diffusivity used.

Also, we can define the poleward heat transport as in [\(10\)](#) for the multiple solutions we obtained under the mixed boundary conditions. For the stable thermal mode, we choose $C_0 = 1/3$ as given in [\(47\)](#); for the haline mode, however, $C_0 = 1/3$ seems to overestimate the poleward heat transport because, unlike the thermal mode in which the convected water can sink to the deep ocean (3000 or 4000 m) and the deep water is nearly homogeneous, the convection can only reach to 1000 m in the haline mode. Thus, the low-latitude-formed “deep” water is a thermocline water mass, and the temperature difference between these waters and the surface return flow is greatly reduced. For simplicity, we choose $C_0 = 1/6$ in the haline mode for the scaling analysis.

For $K = 0.5 \text{ cm}^2 \text{ s}^{-1}$, the results are plotted in [Fig. 8](#). Similar to that under relaxation conditions, the results from numerical experiments are consistent with the scaling analysis. It is obvious that the stable thermal mode transports heat poleward far more efficiently than the haline mode.

4. Discussion and conclusions

From the scaling argument, we conclude that the thermohaline circulation behaves differently under two types of upper boundary conditions. Under “relaxation” boundary conditions, there is only one equilibrium. Under “mixed” boundary conditions, multiple equilibria are possible. The states formed under mixed boundary conditions can be distinguished by a simple relation between the diapycnal diffusivity and the hydrologic forcing for a given thermal forcing. When $K > CE^{3/2}$, there are two thermal modes and one haline mode. When $K < CE^{3/2}$, there is only one haline mode. In addition, through stability analysis, we find that of the two thermal modes arising when $K > CE^{3/2}$, only one is a stable solution. The haline mode solution is always stable.

In the numerical experiments, a two-thirds dependence of meridional overturning on diapycnal diffusivity is obtained under the relaxation boundary conditions. Under mixed boundary conditions, there is an upper limit on the freshwater forcing for a given diapycnal diffusivity beyond which only a haline mode is found. Below that limit we have two modes possible: one thermal mode and one haline mode. The dependence of the critical E on the diapycnal diffusivity also obeys a two-thirds power law given by the scaling argument. Similar scaling dependence is obtained for the poleward heat transport.

The scaling analysis and the numerical experiments are consistent for both types of upper boundary conditions. Thus, it is

reasonable to deduce the lowest order solution using the simple scaling relation. More importantly, in contrast to the box models, we have included the Coriolis parameter, diapycnal diffusivity, and freshwater forcing (for mixed boundary conditions only) in the scaling argument. Under the more physical “mixed boundary conditions,” the sensitivity of the thermohaline circulation to two very uncertain variables, namely, diapycnal diffusivity and freshwater forcing, is defined by an algebraic relation. The importance of E has been previously discussed by [Weaver et al. \(1993\)](#) and others, while the significance of the magnitude of the diapycnal diffusivity to the stability of the thermohaline circulation has not received much attention yet.

Through scaling analysis and simple numerical experiments, the north–south temperature difference, the magnitude of the freshwater forcing, and the diapycnal diffusivity are found to be the most important factors in determining the stability and variability of the thermohaline circulation, of which the latter two are not well known so far. This requires us to develop a much better understanding of these two still challenging fields. The diapycnal (vertical) mixing processes have been under increased observational investigation recently. [Ledwell et al. \(1993\)](#) used a tracer release experiment to estimate a diapycnal diffusivity of $0.1\text{--}0.15\text{ cm}^2\text{ s}^{-1}$ in the upper thermocline, which agrees with the small diffusivity estimates for internal wave processes ([Gregg 1989](#); [Polzin et al. 1995](#)). In contrast, [Toole et al. \(1994\)](#) and [Polzin et al. \(1997\)](#) find that the diapycnal diffusivity in the abyss is far from uniform as traditionally assumed, instead, strong vertical mixing above rough topography can exceed $10\text{ cm}^2\text{ s}^{-1}$, which is two orders of magnitude larger than the thermocline diffusivity found by Ledwell et al. Our analysis indicates that an improved knowledge of both diapycnal mixing and hydrologic forcing is necessary to understand the stability of the thermohaline circulation.

Acknowledgments

We are grateful to John Toole and Jochem Marotzke for comments, suggestions, and conversations. J. Z. and R. W. S. were supported by a grant from the Ocean Sciences Division of the National Science Foundation, OCE94-15589. R.X.H. was supported by NSF through Grant OCE96-16950.

REFERENCES

- Bryan, F., 1986: High-latitude salinity effects and interhemispheric thermohaline circulations. *Nature*, **323**, 301–304.
- , 1987: On the parameter sensitivity of a primitive equation ocean general circulation model. *J. Phys. Oceanogr.*, **17**, 970–985. [Find this article online](#)
- Bryan, K., 1969: A numerical method for the study of the circulation of the world ocean. *J. Comput. Phys.*, **4**, 347–376.
- Cummins, P. F., G. Holloway, and A. E. Gargett, 1990: Sensitivity of the GFDL Ocean General Circulation Model to a parameterization of vertical diffusion. *J. Phys. Oceanogr.*, **20**, 817–830. [Find this article online](#)
- Gent, P. R., and J. C. McWilliams, 1990: Isopycnal mixing in ocean circulation models. *J. Phys. Oceanogr.*, **20**, 150–155. [Find this article online](#)
- Gregg, M. C., 1989: Scaling turbulent dissipation in the thermocline. *J. Geophys. Res.*, **94**, 9686–9698.
- Haney, R. L., 1971: Surface thermal boundary condition for ocean circulation models. *J. Phys. Oceanogr.*, **1**, 241–248. [Find this article online](#)
- Hellerman, S., and M. Rosenstein, 1983: Normal monthly stress over the world ocean with error estimates. *J. Phys. Oceanogr.*, **13**, 1093–1104. [Find this article online](#)
- Hovine, S., and T. Fichefet, 1994: A zonally averaged, three-basin ocean circulation model for climate studies. *Climate Dyn.*, **10**, 313–331.
- Huang, R. X., 1993: Real freshwater flux as a natural boundary condition for the salinity balance and thermohaline circulation forced by evaporation and precipitation. *J. Phys. Oceanogr.*, **23**, 2428–2446. [Find this article online](#)
- , 1994: Thermohaline circulation: Energetics and variability in a single-hemisphere basin model. *J. Geophys. Res.*, **99** (C6), 471–485.
- , and R. L. Chou, 1994: Parameter sensitivity study of the saline circulation. *Climate Dyn.*, **9**, 391–409.
- , J. Luyten, and H. M. Stommel, 1992: Multiple equilibrium states in combined thermal and saline circulation. *J. Phys. Oceanogr.*, **22**, 231–246. [Find this article online](#)

- Ledwell, J. R., A. J. Watson, and C. S. Law, 1993: Evidence for slow mixing across the pycnocline from an open-ocean tracer-release experiment. *Nature*, **364**, 701–703..
- Levitus, S., 1982: *Climatological Atlas of The World Ocean*. NOAA Prof. Paper No. 13, U.S. Govt. Printing Office, Washington, DC, 173 pp..
- Marotzke, J., 1990: Instabilities and multiple equilibria of the thermohaline circulation. Ph.D. thesis, Ber Inst. Meeresk. Kiel, 126 pp. [Available from IFM, Duesternbrooker Weg 20, Kiel D 24105 Germany..]
- , 1997: Boundary mixing and the dynamics of three-dimensional thermohaline circulations. *J. Phys. Oceanogr.*, **27**, 1713–1728.. [Find this article online](#)
- Munk, W. H., 1966: Abyssal recipes. *Deep-Sea Res.*, **13**, 707–730..
- , and C. Wunsch, 1998: Abyssal recipes II, energetics of tidal and wind mixing. *Deep-Sea Res.*, **45**, 1977–2010..
- Pacanowski, R. C., 1995: MOM2 Documentation, User's Guide and Reference Manual. Tech. Rep. 3, GFDL Ocean Group Technical Report, 232 pp. [Available online at [kd/momwebpages/mom.html](http://www.gfdl.gov/~kd/momwebpages/mom.html)].
- Polzin, K. L., J. M. Toole, and R. W. Schmitt, 1995: Finescale parameterizations of turbulent dissipation. *J. Phys. Oceanogr.*, **25**, 306–328.. [Find this article online](#)
- , J. R. Ledwell, and R. W. Schmitt, 1997: Spatial variability of turbulent mixing in the abyssal ocean. *Science*, **276**, 93–96..
- Rahmstorf, S., 1995: Bifurcations of the Atlantic thermohaline circulation in response to changes in the hydrological cycle. *Nature*, **378**, 145–149..
- , J. Marotzke, and J. Willebrand, 1996: Stability of the thermohaline circulation. *The Warm Water Sphere of the North Atlantic Ocean*, W. Krauss, Ed., Gebrüder Borntraeger, 129–158..
- Samelson, R. M., and G. K. Vallis, 1997: Large-scale circulation with small diapycnal diffusion: The two-thermocline limit. *J. Mar. Res.*, **55**, 223–275..
- Schmitt, R. W., 1995: The ocean component of the global water cycle. *Rev. Geophys.*, **33** (Suppl. Part 2), 1395–1409..
- Stommel, H., 1961: Thermohaline convection with two stable regimes of flow. *Tellus*, **13**, 224–230..
- , and A. B. Arons, 1960: On the abyssal circulation of the world ocean. Part II: An idealized model of the circulation pattern and amplitude in oceanic basins. *Deep-Sea Res.*, **6**, 339–343..
- Toole, J. M., K. L. Polzin, and R. W. Schmitt, 1994: Estimates of diapycnal mixing in the abyssal ocean. *Science*, **264**, 1120–1123..
- Warren, B. A., 1983: Why is no deep water formed in the North Pacific? *J. Mar. Res.*, **41**, 327–347..
- Weaver, A. J., and T. M. C. Hughes, 1992: Stability and variability of the thermohaline circulation and its link to climate. *Trends Phys. Oceanogr.*, **1**, 15–70..
- , J. Marotzke, P. F. Cummins, and E. S. Sarachik, 1993: Stability and variability of the thermohaline circulation. *J. Phys. Oceanogr.*, **23**, 39–60.. [Find this article online](#)
- Welander, P., 1971: The thermocline problem. *Philos. Trans. Roy. Soc. London*, **270A**, 415–421..
- Wright, D., and T. F. Stocker, 1992: Sensitivity of a zonally averaged global ocean circulation model. *J. Geophys. Res.*, **97**(C8), 12 707–12 730..

APPENDIX

5. Solution of the Equation $|R^4 - R^3| = F$

Here we solve the above equation in the form of (32) and (33), respectively, to obtain the thermal mode(s) and haline mode solutions.

The quartic equation (32),

$$R^4 - R^3 + F = 0, (A1)$$

can be reduced to solving the following two quadratic equations:

$$R^2 + (-1 + \sqrt{8y + 1})\frac{R}{2} + y\left(1 - \frac{1}{\sqrt{8y + 1}}\right) = 0, (A2)$$

$$R^2 + (-1 - \sqrt{8y + 1})\frac{R}{2} + y\left(1 + \frac{1}{\sqrt{8y + 1}}\right) = 0, (A3)$$

where y is the arbitrary root of the following cubic equation:

$$y^3 - Fy - \frac{F}{8} = 0. (A4)$$

It is readily shown that, when $F < 27/256$, there are two solutions to (A2)–(A3). When $F > 27/256$, no thermal mode is possible. Thus, the criteria $F = 27/256$ determines the existence of thermal modes.

Similarly, for Eq. (33), and it can be derived that there is always one and only one haline mode solution given any external conditions.

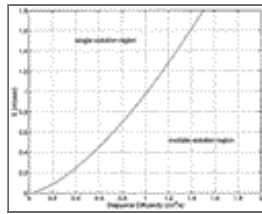
Tables

Table 1. Comparison of the North Atlantic and North Pacific Oceans.

	North Atlantic	North Pacific
L_r (10^6 m)	6	12
ΔT ($^{\circ}\text{C}$)	18	20
\bar{S} (psu)	36	34
K ($\text{cm}^2 \text{s}^{-1}$)	1	1
E_c (m yr^{-1})	0.92	0.89
E (m yr^{-1})	0.75	1.05
Mode	Multiple	Haline

[Click on thumbnail for full-sized image.](#)

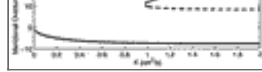
Figures



[Click on thumbnail for full-sized image.](#)

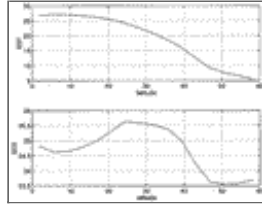
Fig. 1. Critical curve $F_c = 27/256$ with the parameters as $\alpha = 2.0 \times 10^{-4} \text{ K}^{-1}$, $\beta = 8.0 \times 10^{-4} \text{ psu}^{-1}$, $\Delta T = 20 \text{ K}$, $\bar{S} = 35 \text{ psu}$, $f = 1.0 \times 10^{-4} \text{ s}^{-1}$, $L = 6.0 \times 10^6 \text{ m}$, and $g = 9.8 \text{ m}^2 \text{ s}^{-1}$. In the region below the critical curve, three modes are possible: two thermal modes and one haline mode, while in the region above it, only one haline mode can exist.





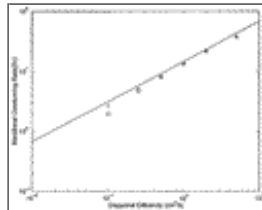
Click on thumbnail for full-sized image.

Fig. 2. Solutions of meridional overturning rate under mixed boundary conditions for (a) fixed $K = 1.0 \text{ cm}^2 \text{ s}^{-1}$ with changing E and (b) fixed $E = 1 \text{ m yr}^{-1}$ with changing K . The upper solid line corresponds to the stable thermal mode, while the lower solid line is the solution for the haline mode, and the dotted line represents the result for the unstable thermal mode. For $K = 1 \text{ cm}^2 \text{ s}^{-1}$, there is a bifurcation point at about $E = 1 \text{ m yr}^{-1}$, beyond which only one haline mode is possible. The parameters are defined in [Fig. 1](#).



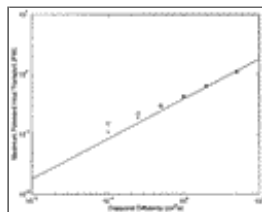
Click on thumbnail for full-sized image.

Fig. 3. The prescribed SST and SSS fields for the experiments under relaxation boundary conditions. Here we have approximately $\Delta T = 20 \text{ K}$ and $\Delta S = 2 \text{ psu}$.



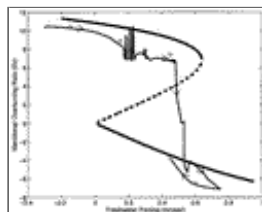
Click on thumbnail for full-sized image.

Fig. 4. Meridional overturning rate from scaling analysis and numerical experiments under relaxation boundary conditions. The “x” and “o” represent the numerical results without and with wind stress, respectively. The solid line represents the scaling argument results, where the meridional overturning rate is proportional to the two-thirds power law of diapycnal diffusivity, with $\Delta S = 2 \text{ psu}$ and other parameters the same as in [Fig. 1](#).



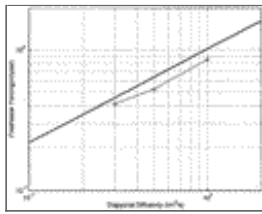
Click on thumbnail for full-sized image.

Fig. 5. Poleward heat transport from scaling analysis and numerical experiments under relaxation boundary conditions. The “x” and “o” represent the numerical results without and with wind stress, respectively. The solid line represents the scaling argument results, where the poleward heat transport is proportional to the two-thirds power law of diapycnal diffusivity and with parameters the same as in [Fig. 4](#).



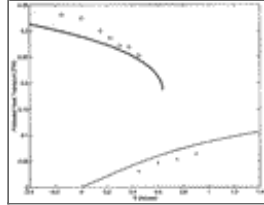
Click on thumbnail for full-sized image.

Fig. 6. Meridional overturning rate from scaling analysis and numerical experiments under mixed boundary conditions with $K = 0.5 \text{ cm}^2 \text{ s}^{-1}$. Here the thick lines represents the results from scaling analysis, the line with arrows is the response of the numerical model to the very slowly changing freshwater forcing, and the circles represent the single numerical experiments for different E forcing. Arrow directions represent the freshwater change with time in the process of integration. No wind stress is applied in this experiment.



Click on thumbnail for full-sized image.

Fig. 7. Critical freshwater from scaling analysis and numerical experiments under mixed boundary conditions. The solid line is for scaling results and the circles are from the hysteresis numerical experiments.



Click on thumbnail for full-sized image.

Fig. 8. Poleward heat transport from scaling analysis and numerical experiments under mixed boundary conditions. The solid lines are for scaling results (heavy line for the stable thermal mode and thin line for the haline mode), “○” are from the numerical experiments in the thermal mode, and “×” are for numerical experiments in the haline mode. For all the numerical experiments and the scaling argument, $K = 0.5 \text{ cm}^2 \text{ s}^{-1}$.

* WHOI Contribution Number 9518.

+ Present affiliation: The North Bridge Group, Lincoln, Massachusetts.

Corresponding author address: Raymond W. Schmitt, MS21, Department of Physical Oceanography, Woods Hole Oceanographic Institution, Woods Hole, MA.

E-mail: rschmitt@whoi.edu

top ▲



© 2008 American Meteorological Society [Privacy Policy and Disclaimer](#)
 Headquarters: 45 Beacon Street Boston, MA 02108-3693
 DC Office: 1120 G Street, NW, Suite 800 Washington DC, 20005-3826
amsinfo@ametsoc.org Phone: 617-227-2425 Fax: 617-742-8718
[Allen Press, Inc.](#) assists in the online publication of AMS journals.